JOHN R. APEL and DAG T. GJESSING

INTERNAL WAVE MEASUREMENTS IN A NORWEGIAN FJORD USING MULTIFREQUENCY RADARS

A joint United States–Norway internal wave experiment was carried out in the Sognefjord, Norway, in July 1988. The experiment used coherent, multifrequency delta-k radars to observe internal waves generated by a ship in the stratified waters of the fjord. By matching the radar interference or beat wavelength to the scales of the internal waves, enhanced detectivity of the waves was obtained.

INTRODUCTION

Delta-k Radar

The concept of matched illumination of targets using coherent multifrequency radars has been advanced by several authors[1,2] as a means of enhanced detection and identification of objects. The simultaneous (or near-simultaneous) transmission of two coherent electromagnetic waves at frequencies f_1 and f_2 can be considered to develop a spatial interference, or "beat," pattern along the transmission path. The distance between nulls in the interference pattern can be made to vary over a wide range of scales with relatively small changes in transmitted frequencies. If $\Delta f_{21} = f_2 - f_1$ is the difference frequency and c is the speed of light, then the interference scale L is

$$L = \frac{c}{2\Delta f_{21}} .$$

A target whose characteristic longitudinal dimensions include sizes near L is believed to backscatter the incident radiation resonantly. A nonlinear detector receiving the scattered radiation will generate sum and difference frequencies, and narrowband post-detection filtering will observe this enhanced backscatter at the difference frequency Δf_{21}, while rejecting out-of-band noise.[3]

If n closely adjacent frequencies are transmitted simultaneously, then $n(n-1)/2$ pairwise difference frequencies, Δf_{ij}, will be formed in the detector. If a given target has spatial Fourier components that match several of the "difference wavelengths,"

$$L_{ij} = \frac{c}{2\Delta f_{ij}} , \qquad i, j = 1, \ldots, n; \qquad i \neq j ,$$

it will backscatter the incident radiation in each matching channel. Narrowband post-detection filtering can again increase the signal-to-noise ratio. Because the frequencies are all coherent, the possibility also exists of further processing gain via coherent integration of all of the pairwise combinations. Theoretical studies by Gjessing et al.[3] indicate that up to 68 dB of processing gain (relative to receiver noise) can be obtained from a six-frequency C-band system for which 15 difference frequencies can be formed. Figure 1, a schematic of a pair of interfering radar waves incident on the ocean surface at a large incidence angle, θ_i, illustrates the scale-matching concept.

All of these concepts have been tested on hard targets such as aircraft, where the scale-matching was made on characteristic target dimensions such as fuselage length, wingspan, engine nacelle spacing, etc. They have also proven to be efficacious in determining ocean surface wave spectra, or at least the line-of-sight components thereof. One of the more useful radar parameters in this regard is the Doppler spectrum of target scatters.

Single-Frequency Doppler Spectra

If the target moves at a line-of-sight velocity v, a Doppler shift will be introduced on each of the backscattered signals and is given by

$$\delta f_i = 2 f_i \frac{v}{c} , \qquad i = 1, \ldots, n .$$

A measurement of the Doppler shift at each frequency determines the line-of-sight velocity component of the scatterer. For a relatively rigid target such as an aircraft, all of the scattering centers on the target are moving with the same mean velocity. The magnitudes of the Doppler shifts are proportional to the carrier frequencies f_i, and the Doppler spectrum therefore consists of a narrow line centered at $2f_i v/c$. Any vibration, rotation, or torsion will broaden the Doppler lines and increase their widths, and the broadening will be a measure of the differential motions within the target. On an aircraft, the flutter frequencies of control surfaces appear as a spreading of the basic carrier line in the Doppler spectrum of such a target.

Scattering from Oceanic Surface and Internal Waves

If the target is a distributed structure (such as a patch of ocean surface) instead of a rigid structure, each Fourier component of the wave spectrum will move with its own velocity. A measurement of the velocity-induced

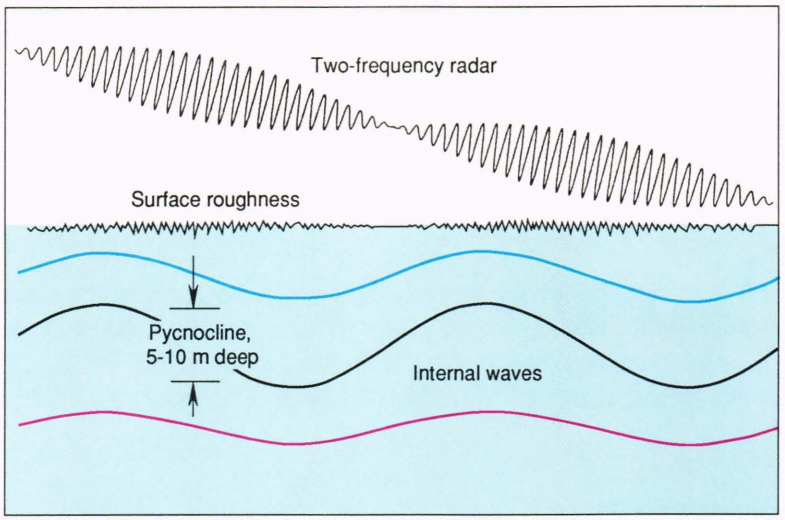

Figure 1. Schematic of two-frequency delta-k scale matching. Internal waves modulate short gravity waves, and the resultant roughness scales scatter electromagnetic radiation when the interference scale matches the roughness scale. (Illustration provided by the Norwegian Environmental Surveillance Program, Royal Norwegian Council for Scientific and Industrial Research.)

shifts and broadenings within an illuminated area will then determine the Doppler spectrum of the scattering elements. For large incidence angles, θ_i, the ocean acts as a random diffraction grating, and the dominant backscatter mechanism is Bragg scatter. Then, the centroid of the Doppler spectrum will appear near the frequency of the Bragg waves, that is, those waves that satisfy the relationship

$$k_b = 2\pi/\lambda_b = 2k_r \sin\theta_i \ .$$

Here, λ_b is the wavelength of the ocean wave spectral component that causes Bragg scatter of electromagnetic radiation of wavelength $\lambda_r = 2\pi/k_r$.

At smaller (steeper) incidence angles, specular points on the ocean surface begin to contribute to the backscatter. The small, specularly scattering wave facets riding on longer gravity waves will cause a much higher level of backscatter from the side of the waves facing toward the radar than from the side facing away from it. Consequently, the average power from the front face of a wave traveling toward the radar will be greater than that from the back face; in this case, the net Doppler shift will be positive. (The Bragg scattering will also be higher from the area tilted toward the normal.) This effect distorts the Doppler spectrum and complicates its interpretation; however, existing theories adequately account for the effect (see the article by Thompson elsewhere in this issue).

For ocean surface gravity waves propagating in a current system moving at velocity **U**, the dispersion relation is

$$\omega = \omega(\mathbf{k}_b) = \mathbf{k}_b \cdot \mathbf{U} \pm \sqrt{gk_b} \ ,$$

where the first term is the Doppler shift caused by currents through which the waves are moving and the second term is the intrinsic gravity wave dispersion. The presence of a larger-scale mean current, **U**, also complicates the scattered spectrum by causing an additional net Doppler shift, δf_u, on the backscattered frequencies given by

$$\delta f_u = \mathbf{k}_b \cdot \mathbf{U}/2\pi \ .$$

If there are spatially varying large-scale currents within the radar footprint, each element of current will contribute its own shift and backscattered power. In a wideband process such as ocean surface wave propagation, there is a broad distribution of scattering elements and currents, and the actual spectrum is significantly spread out by the variability present. Thus, the Doppler spectrum is a complicated functional of the ocean wave amplitude and velocity distributions. These spectra have been the subject of much study.

Figure 2 is a schematic illustration of a C-band Doppler spectrum from ocean surface waves for an approaching gravity wave system propagating through a positive (approaching) current. The angle of incidence is taken to be large enough (typically greater than 25° to 30°) so that only Bragg scatter obtains, with no contribution from specular point scatter.

For internal waves, the dispersion equation is somewhat more complicated than for surface gravity waves and cannot generally be written out explicitly, in contrast with the case for surface waves. It is, however, a monotonically increasing function of wave number. A simple generic model for $\omega = \omega(k_i)$ for internal waves is given by

$$\omega = \omega(k_i) = N_0 \frac{k_i c_0}{N_0 + k_i c_0} \ .$$

(Barber, B. C., personal communication [1988]). This formula demonstrates the characteristic behavior of internal waves at low frequencies, where the phase speed ω/k_i approaches c_0 (the long-wave phase speed), as well as the asymptotic behavior at high frequencies when ω approaches N_0, the so-called Brunt–Väisälä or buoyancy frequency (the maximum frequency at which an internal wave can oscillate). The Brunt–Väisälä fre-

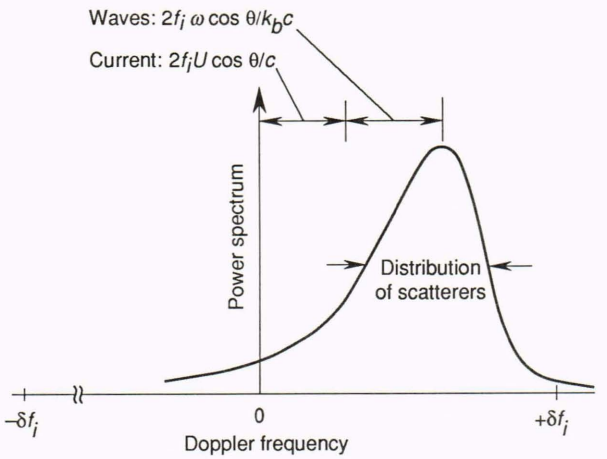

Figure 2. Schematic of a single-frequency Doppler spectrum showing contributions from both short surface wave Bragg scatterers and current-induced advection.

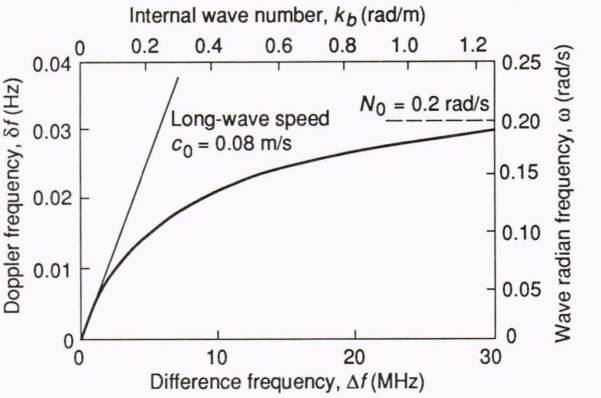

Figure 3. Dispersion relation for lowest-mode internal waves in the Sognefjord, with legends for both hydrodynamic scales and delta-k scales.

quency is set by the logarithmic derivative of the vertical water density profile, $\rho(z)$:

$$N_0 = \sqrt{-\frac{g}{\rho}\frac{\partial\rho}{\partial z}} \quad .$$

Here, g is the acceleration of gravity, and the vertical coordinate, z, is positive upward. An example of the actual dispersion relation for the lowest-order wave mode in the Sognefjord is shown in Fig. 3 for zero mean velocity, U. Although a denumerable infinity of quantized vertical modes for internal waves exists (not shown in Fig. 3), usually only the lowest-order modes are excited by a surface ship.

Delta-k Doppler Spectra

Until now, the discussion of spectra has been in terms of single-frequency processing, rather than delta-k processing. However, a Doppler spectrum can be calculated for each delta-k channel as well as for the carrier. Ocean waves scatter electromagnetic waves that impinge upon them; at typical radar frequencies, the single-frequency Doppler shifts are in the range of tens to hundreds of hertz. However, the difference wavelengths associated with ocean waves, L_{ij}, are typically 150 to 1.5 m, and the difference frequencies are on the order of 1 to 100 MHz, so that the Doppler shifts of the delta-k channels are reduced from those of the carrier channels by approximately the ratio $\Delta f_{ij}/f_i$. The difference wave numbers are proportional to the difference frequencies, meaning that a plot of the delta-k Doppler shifts versus the difference frequency is a mapping of the ocean wave dispersion relation, $\omega = \omega(\mathbf{k}_b)$, into a space measured by δf_i and Δf_{ij}. For surface gravity waves observed in the delta-k mode, a relationship results between Doppler and difference frequencies that is given by

$$\delta f_i = 4\pi\Delta f_{ij} U_l/c \pm \sqrt{4\pi g\Delta f_{ij}/c} \quad .$$

Here, U_l is the line-of-sight velocity component between the radar propagation vector and the current vector.

Jensen discusses delta-k processing and the associated Doppler spectra elsewhere in this issue.

OVERVIEW OF THE EXPERIMENT

Objectives

An experiment conducted under the scientific direction of APL and the Norwegian Environmental Surveillance Program in the summer of 1988 tested the delta-k concepts on internal waves. Called the U.S.–Norway Ocean Radar Project, it was co-sponsored by the Defense Advanced Research Projects Agency and the Royal Norwegian Council for Scientific and Industrial Research. The project was intended to establish the first-order capabilities of multifrequency radars to discern variations in backscatter from the ocean surface caused by processes such as internal waves and wind roughening. The experiment addressed the basic physics and engineering issues associated with detecting backscatter modulations, especially from internal waves, and was carried out in an environment selected to optimize the detectability of such modulations.

The following were specific objectives:

1. Conduct an experiment in a Norwegian fjord, observing man-made surface signatures of internal wave wakes to establish the approximate capabilities of multifrequency radars for detecting internal waves.
2. Characterize the environment sufficiently well to obtain a quantitative understanding of the subsurface and surface hydrodynamics on the scales of interest.
3. Apply and modify existing theories of electromagnetic backscatter modulations and their detectivity to the data obtained from the fjord at both microwave and optical frequencies.
4. Establish the approximate radar parameters required to detect the internal waves and other backscatter modulations with maximum signal-to-noise ratio.

Description

The experiment was carried out in the Sognefjord in south-central Norway in late June and early July 1988. The site was near the junction of the Sognefjord and the Aurlandsfjord (Fig. 4), a region deep within the Sognefjord. The fjord is unaffected by internal and surface waves of oceanic origin, although there is a tidal excursion of about 1 m in the area. In early to midsummer, the region is characterized by the presence of a thin (5-m) isohaline layer of brackish water overlying much deeper salt water (900 m); the brackish water results from a mixing of seawater and snow-melt runoff, which occurs only during a limited time each year. There is also a deeper thermocline, on the order of 7 to 8 m thick, which, together with the halocline, establishes the density profile (pycnocline), an example of which is shown in Figure 5. The experiment was conducted by using a wave-making ship, two research vessels, two delta-k radar installations on the mountainside of the fjord, and two additional radars emplaced on a gondola suspended from a deactivated high-voltage transmission line spanning the fjord.

The radars were C-, X-, and W-band devices. The C-band system, which belonged to the Norwegian Environmental Surveillance Program, transmitted interrupted continuous-wave (CW) signals at six frequencies centered near 6.8 MHz. The X-band system, owned by Metratek, Inc., was a stepped-frequency system that transmitted a train of coherent submicrosecond pulses whose frequency differences—and hence delta-k wavelengths—were designed to match short-wavelength scales in the internal wave field. Both Norwegian and U.S. radars operated from the hillside about 800 m above the fjord and viewed the experimental area at incidence angles near 60°.

An additional pair of Norwegian radars was located on the gondola. The C-band system, a lightweight duplicate of the hillside system, operated as an interrupted CW radar at 4.5 GHz. The W-band radar, a 96-GHz pulsed system, functioned mainly as a coherent scatterometer. Incidence angles for both ranged between 10° and 50°. The gondola, which was between 150- and 300-m elevation (depending on the incidence angle desired), provided these radars with an excellent site from which to make radar backscatter measurements of the water's surface, especially at steeper angles, without the usual wave disturbances from the hull of a ship or from ocean tower pylons. Figures 6 and 7 show the plan and profile views, respectively, of the experimental arrangement.

Besides the hillside and gondola radars, several video systems were in operation for documentation of ship movements, surface conditions, etc. Instrument-quality high-resolution video data were provided by APL for scientific use. An extensive array of *in situ* instrumentation was installed on the research vessels *H. V. Sverdrup*, a Royal Norwegian Navy ship, and *Osterøy*, a privately owned vessel. The *Sverdrup* was used to emplace moorings and buoys and to make subsurface and surface hydrodynamic measurements. The hydrodynamic instrumentation on the *Sverdrup* was fielded by the Norwegian Hydrotechnical Laboratory and APL. The *Osterøy* carried a sophisticated instrumentation array belonging to TRW, Inc., that included a laser for measuring small-scale surface slope spectra, a radar for coherent backscatter measurements at X and K bands, and instruments for determining surface and internal wave characteristics.

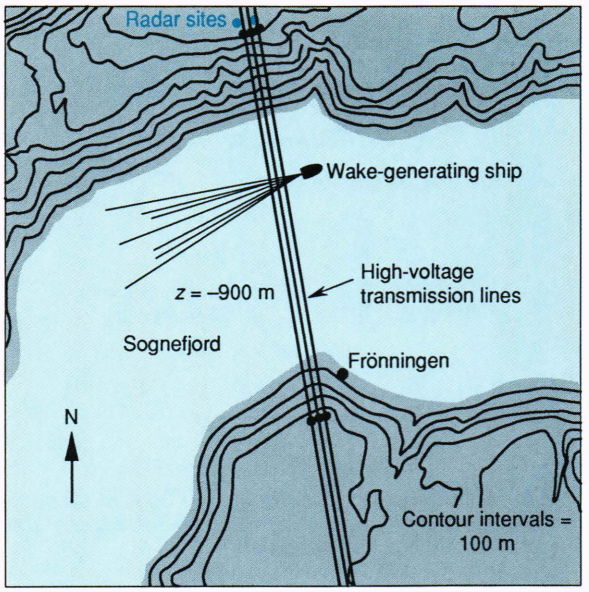

Figure 4. Map of the Sognefjord region in southwestern Norway. The experiment was conducted under high-voltage wires crossing the fjord. Radar measurements were made from both the mountainside and from a gondola on the deactivated high-voltage lines.

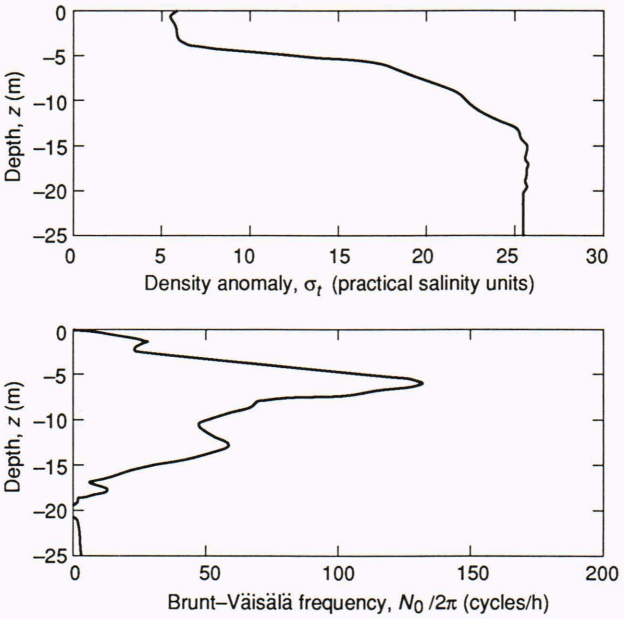

Figure 5. Profiles of density and buoyancy frequency for the Sognefjord. During conditions of spring snow melting, a thin layer of lighter, fresher water overlies the deeper salt water. (Illustration provided by the Norwegian Hydrotechnical Laboratory.)

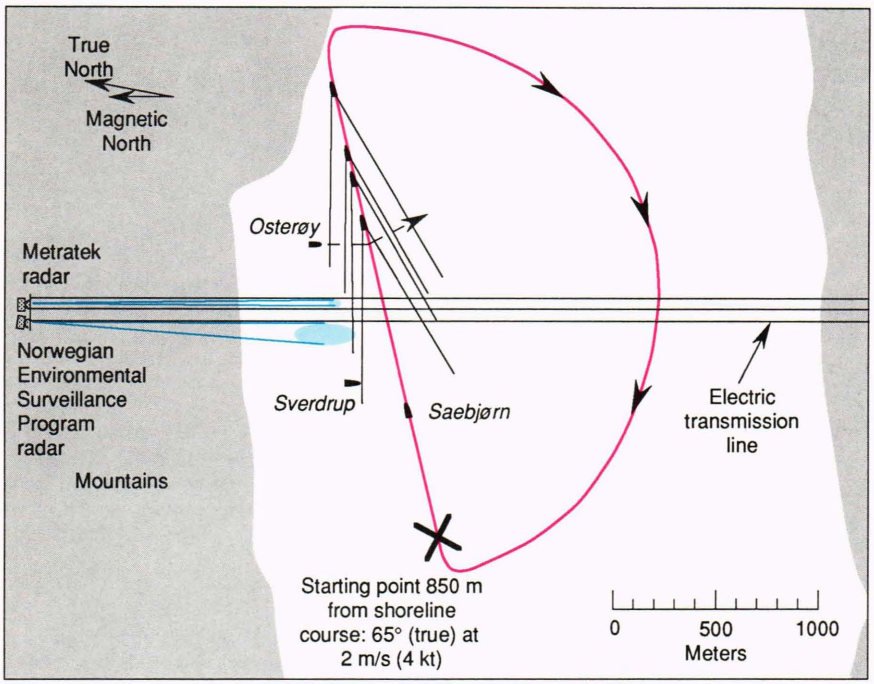

Figure 6. Plan view of the experiment, showing ship course and radar footprints. The wave-making ship was the *Saebjørn*, and the research vessels were *Sverdrup* and *Osterøy*.

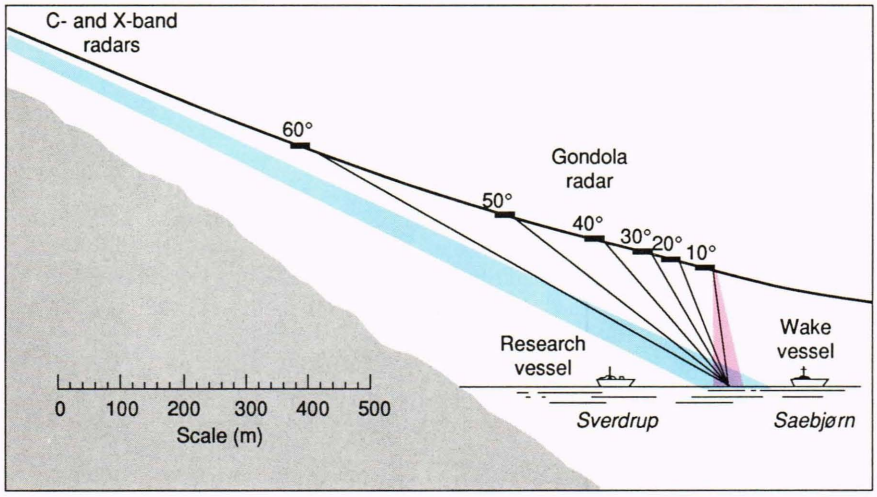

Figure 7. Profile view of the experiment, showing incidence angle variations available from the gondola and from the mountainside. The gondola allowed steep incidence angles without perturbations from a measurement vessel or ocean platform.

Surface ships in the fjord make internal wave wakes that are readily visible to the eye and to cameras. The cover of this issue is a photograph of the Sognefjord on 7 July 1989 showing the wake-generating vessel and its strong internal wave wake signature. This signature is caused by surface roughness variations predominantly in the wavelength range of 1 to 2 m. Well-configured imaging or nonimaging radars can detect such features via backscatter modulations because of variations in surface wave roughness accompanying the internal waves. At the incidence angles used in the experiment, the basic backscatter mechanism is Bragg scatter. Under moderate wind conditions, ample near-equilibrium surface wave energy exists at the Bragg wavelengths of the radars (nominally 1 to 10 cm), so that strain caused by the internal currents modulates the Bragg waves by roughly 20% or more. Such modulation requires surface current strain rates, $(\partial u/\partial x)_{z=0}$, on the order of 5×10^{-3} s^{-1}, which occur in an internal wave field of 50-m wavelength and 50-cm amplitude. Such a short-scale field was readily set up by a ship of about 6-m draft and about 50-m length moving over the pycnocline at a speed near 2 m/s.

Observational Results: Subsurface and Surface Hydrodynamics

Because instrumentation measures only point values of the three-dimensional, time-dependent hydrodynamic field, theory and models must be used to derive the quantities of interest from the data. We first discuss the internal wake properties as deduced via this method.

Keller and Munk[4] developed a kinematic theory for the generation of internal waves in a stratified fluid by a surface ship. As further developed by Dysthe and Trul-

sen (see their article elsewhere in this issue), the source-sink theory of internal wave wake generation predicts the wake pattern in the horizontal plane shown in Figure 8 for supercritical Froude number flow. The outermost crest of the internal wake has an angle with respect to the centerline, ϕ_0, given by

$$\phi_0 = \sin^{-1}(c_0/V) ,$$

where c_0 is the infinite-wavelength internal wave speed and V is the ship speed. For values of $c_0 \approx 0.8$ m/s (as calculated from the observed density profiles) and for $V = 2$ m/s, $\phi_0 \approx 23°$. This angle is not, however, that of the first *observable* wake arm, which occurs near the location of the first maximum downward displacement. The curves ψ = constant give the lines of constant wave phase. The curve $\psi = 2\pi$ in Figure 8, which lies inside the region of maximum strain, gives the horizontal locus of the first zero crossing of the amplitude. The region of maximum strain rate lies approximately one-half to three-fourths of the local wavelength outside the $\psi = 2\pi$ curve, and that region is presumed to have the maximum surface roughness.

Figure 12 in the Dysthe and Trulsen article (elsewhere in this issue) shows the eigenfunctions for the first two internal wave modes, whose associated dispersion relation is that of Figure 3 in this article. The ship-wake waves generally lie in the dispersive, curved portion of the latter diagram. Their Figures 11 and 13 illustrate modeled horizontal and vertical currents (u, v, and w) as derived from the theoretical model.

The 51-m-long *Saebjørn* generated multiarm internal wave wakes with a half-angle of about 17° for the leading crest and with decreasing angles interior to the wake arm. The visible surface signatures persisted for at least 2 km behind the ship (the run geometry prohibited generation of longer crests). The peak-to-trough amplitude of the internal waves, as measured approximately 800 m behind the ship at a depth of 4.7 m, was about 1.5 m. No Kelvin wake is visible at these low speeds. Figure 9 shows the vertical component of internal wave wake current as measured by ultrasonic current meters at a depth of 4.7 m.

Surface wave observations made by TRW were of two general types: (1) The laser slope gauge yielded wave-slope spectra for wave numbers, k_x, along the propagation direction of the internal waves; we denote these fine-grained measurements by $S_\xi(k_x)$, where ξ is the surface wave slope. (2) A wave-height capacitance gauge gave the temporal behavior of wave heights near the region of radar observations and allowed the calculation of surface-wave-height frequency spectra, $S(\omega)$. The laser slope gauge gives the component of surface slope spectra in the x-direction (internal wave propagation direction) for wavelengths from approximately 0.20 m to 3 mm. Coincident with the laser measurements, the TRW observatory determined several other variables: the longer components of the surface wave spectra via a three-wire capacitance gauge; internal wave amplitudes via a subsurface, 200-kHz echo-sounder; and X-band radar backscatter at 40° incidence angle, for both polarizations, from the same region of water surface being scanned by the laser. Figure 10 illustrates the average surface-wave slope spectrum for Run 4 on 12 July 1988. Over a range of wave numbers from approximately 0.33 to 3.0 cm^{-1}, the slope spectrum obeys a power law close to $S_\xi(k_x) \sim k_x^{-3.2}$. The roll-off at lower wave numbers results from the limits on the size of the region scanned by the laser. The peaks at higher wave numbers are artifacts of the instrumentation; the high-frequency response is limited by the measurement of laser beam position at the detector.

Time series of the surface wave heights obtained from the APL spar buoy show that the dominant wind-driven

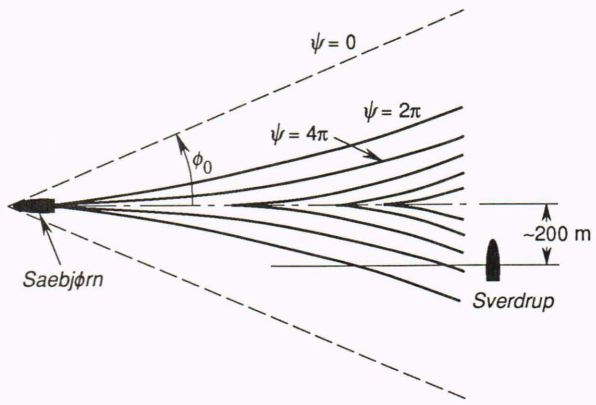

Figure 8. Horizontal pattern of internal wave constant-phase lines, showing the position of the measurement ship, *Sverdrup*. The first visible wake arm lies approximately one-fourth of the distance between $\psi = 0$ and $\psi = 2\pi$. (Illustration provided by the Norwegian Environmental Surveillance Program and the University of Tromsø.)

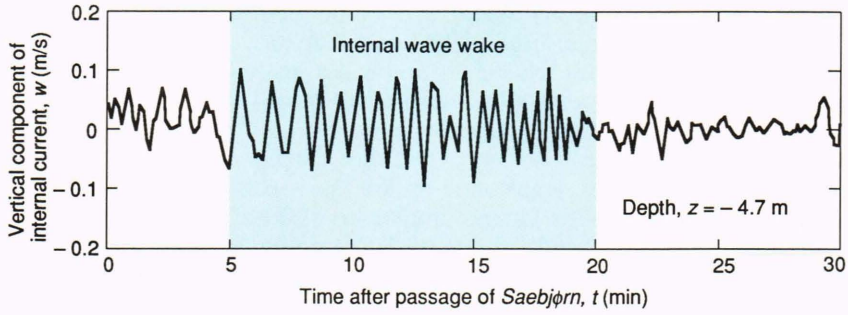

Figure 9. Vertical component of internal currents induced by the *Saebjørn* at a depth of 4.7 m. The distance from the *Saebjørn* track is 200 m. (Illustration provided by the Norwegian Hydrotechnical Laboratory.)

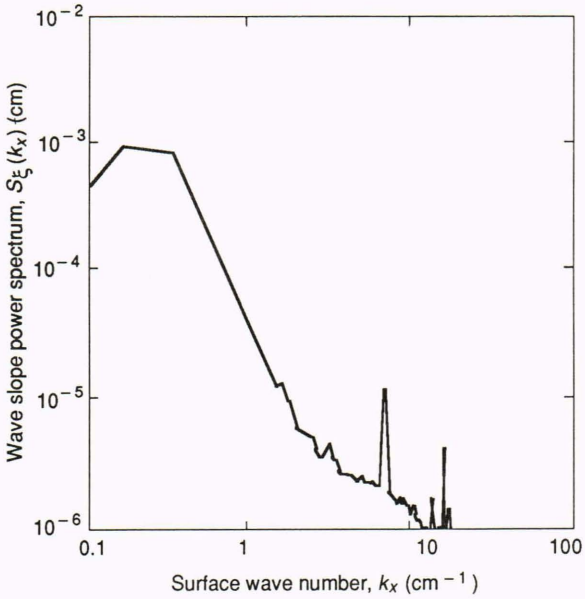

Figure 10. Surface-wave slope spectrum from the TRW laser slope gauge. The gauge can resolve gravity/capillary waves between approximately 0.20 m and 3 mm. The high-frequency peaks are artifacts. (Illustration provided by TRW, Inc.)

surface waves have periods near 2.5 s. In addition to the surface waves, the internal wave motions also appear in the time series. Because of fluid drag and buoyancy changes exerted on the spar buoy by the internal waves, vertical oscillations starting at periods near 70 s and descending to 30 s are impressed on the buoy. The phasing of the surface and internal wave signals shows that the surface waves are statistically stronger near the descending part of the internal waves. The data also show that the surface waves accompanying the internal waves are quite coherent, have periods near 1.3 s (wavelengths near 1 m), and have peak-to-trough amplitudes on the order of 0.2 m. These waves are resonant with the internal wave phase speeds and can therefore exchange energy with the waves to the greatest extent. The resonance requirement is approximately that the group speed of the surface waves, c_g, be equal to the phase speed of the internal waves, c_i. For deep-water surface gravity waves, $c_g = 0.5\, c_\phi$, where c_ϕ is the surface wave phase speed, and the resonance requirement can be written as

$$c_i \approx c_g = \tfrac{1}{2}\, c_\phi = \tfrac{1}{2} \sqrt{g\lambda/2\pi} \quad .$$

For both natural and man-made internal waves, the phase speeds quite often fall in the range of about 0.4 to 0.8 m/s. It then follows that the wavelengths of the resonant surface waves (after speed changes and refraction by the internal currents through which they travel to arrive at a region of resonance) will generally fall in the range of about 0.4 to 1.6 m. This range is observed in the present experiment.

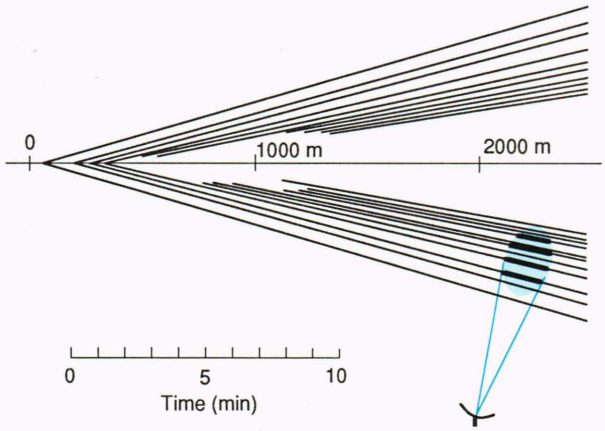

Figure 11. Delta-k matched illumination to internal wave crests showing how the internal wake is sampled by the delta-k radar footprint. Water wavelengths and frequencies are effectively "chirped" during ship passage. (Illustration provided by the Norwegian Environmental Surveillance Program.)

Observational Results: Radar Scattering

Single-Frequency Results. The geometry of the experiment (Fig. 6) was such that with a given radar footprint, the ship internal-wave wake arms first entered the beam pattern a few minutes after the ship passed, slowly crossed the beam, and then exited after approximately 15 min. Power scattered from the water surface is approximately centered on the frequency of the Bragg waves but is broadened by the distribution of scatterers in the wave field. Both advancing and receding waves contribute to the Doppler spectrum. The internal waves are seen as an enhancement of the backscattered power during their passage because of the extra roughness accompanying them.

Delta-k Results. Figure 11 shows how the delta-k illumination can be regarded as a time- and space-dependent matching process. The ship internal wake has low spatial frequencies in the outer part of the arms that rapidly increase to higher values closer to the centerline (Fig. 8). Similarly, a cut through the pattern at constant distance from the centerline generates a time-varying signal that sweeps upward in frequency (Fig. 9). Thus, the wake may be regarded as being "chirped" in both space and time.

As discussed earlier, the delta-k matched illumination can be regarded as undergoing scatter from a kind of surface-wave diffraction grating at the difference wavelengths $L_{ij} = c/2\Delta f_{ij}$. As the wake moves past the radar footprint, different members of the 15 beat wavelengths will scatter from the wake arms at different times, resulting in the spatially integrated signal from all waves within the footprint being a complicated function of time. Figure 12, a theoretical mapping of the intensity of backscatter versus time, shows how various wave number components resonate with the wake as it passes through the radar footprint.

As with the single-frequency case, it is possible to calculate two-sided Doppler spectra of the complex, time-

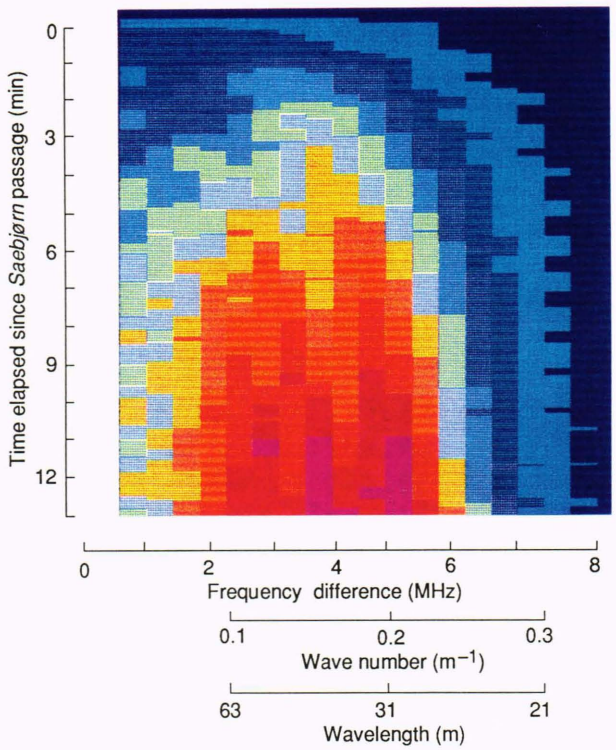

Figure 12. Backscattered delta-k power variations in time and wave number as the internal wave progresses through the beam. At any one time, a variety of spatial scales contributes to the integrated power. (Illustration provided by the Norwegian Environmental Surveillance Program.)

dependent delta-k signals. Figure 13 shows the detector output for Run 3 on 7 July for 6 of the 15 difference frequencies, plus total power (the bottom curve). The inserts give the delta-k Doppler spectra for those signals. Note that only the lower difference frequencies show appreciable power. Each of these time series can be Fourier transformed to obtain a Doppler spectrum. Figure 14 shows spectra for the four lowest frequencies of 2.0, 2.5, 5.0, and 7.0 MHz, as constructed from 2-min segments of the data of Figure 13 starting at 1408:30 European Summer Time. The central peak in the first three of these plots is the delta-k resonance signal, which is quite narrow, but as Δf increases, there are increasing amounts of off-resonance noise. At 7.0 MHz, the spectral estimate is quite noisy, and no peak can be identified as coming from the wake. Note the narrow range (± 0.1 Hz) of Doppler frequencies in the plots. The peaks are quite sharp, with widths of less than 0.01 Hz. To resolve such narrow lines requires at least 100 s of stable data. These data, in principle, demonstrate the resolving power and signal-to-clutter ratio available with a delta-k implementation.

Figure 15 shows a plot of the positions of the three resonant peaks in the Doppler spectra of Figure 14 (the data points) versus the difference frequencies, Δf_{ij}, for the hillside C-band radar. Also plotted in the figure is the dispersion relation for internal waves. Because each wavelength within the internal wake moves with its own velocity, the delta-k Doppler shifts measure the line-of-

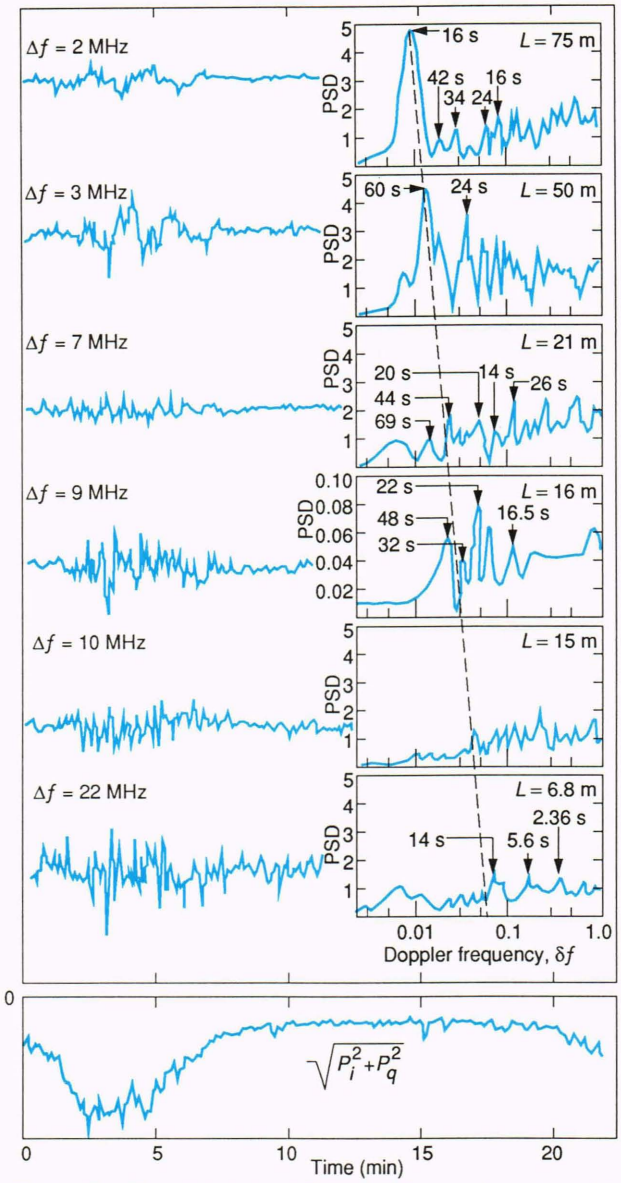

Figure 13. Time variations of C-band difference frequency signals for 6 of 15 delta-k's (left), plus total power at single frequency (bottom); spectra of time series show narrow peaks at low Δf where matching occurs, and broadband noise at $\Delta f \geq 7$ MHz (right). In the upper part of the figure, the ordinate is receiver voltage; in the lower, receiver power (both are in arbitrary units). The dashed line in the upper right is the line of constant velocity; PSD denotes the power spectral density. (Illustration provided by the Norwegian Environmental Surveillance Program.)

sight component of the wave phase velocity. The projection of the difference wavelength onto the water surface measures the wavelength of the resonant internal wave. This constitutes a mapping of the wave (ω, k_i) dispersion relation into the Doppler frequency–difference frequency space. The agreement between these two completely independent measures of dispersion, one electromagnetic and the other hydrodynamic, is considered to be very good. Even better agreement for the 4.5 GHz system is shown in Figure 9 of Jensen's article elsewhere in this issue.

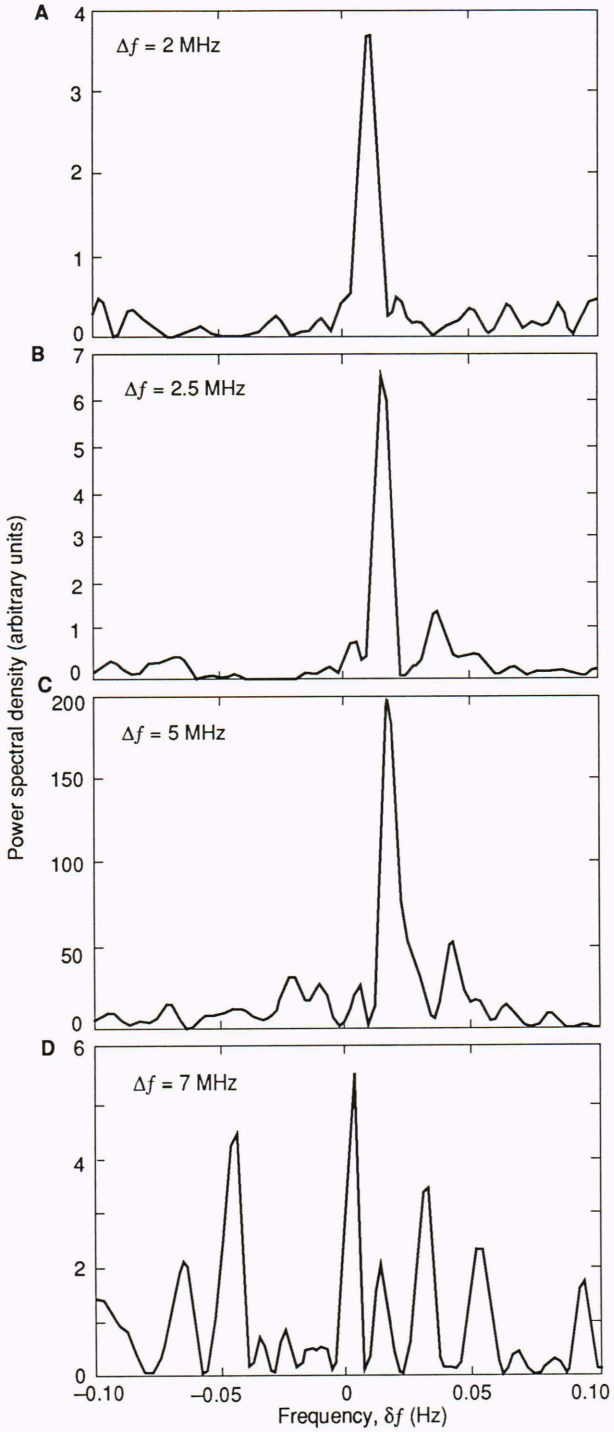

Figure 14. Doppler spectra for four C-band difference frequencies, Run 3, 7 July 1988. The first three plots, for which Δf = 2.0, 2.5, and 5.0 MHz, show clear resonance peaks arising from matched illumination of internal waves; the fourth, for Δf = 7.0 MHz, is quite noisy.

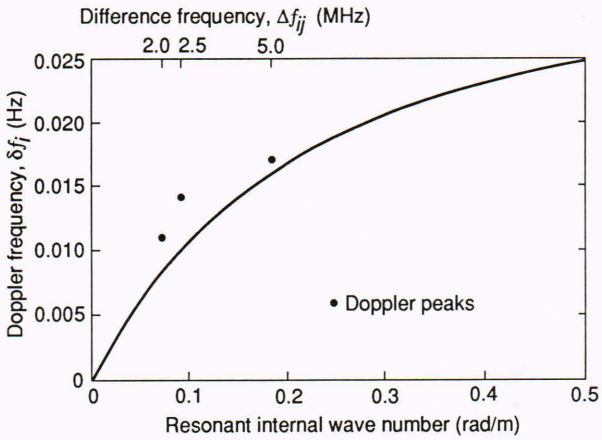

Figure 15. Peaks of three delta-k Doppler spectra from Figure 13 superimposed on the internal wave dispersion relation. Agreement is quite good between completely independent electromagnetic and hydrodynamic measurements.

The Metratek X-band radar is a significantly different device from the Norwegian Environmental Surveillance Program instrument. Termed a pulsed-delta-k (PDK) system, it works by transmitting a train of short pulses, each differing in frequency from the previous one by the desired amount. Pulse lengths can be made as short as 20 ns, which is equivalent to a spatial resolution of 3 m. As long as neither the transmitter nor the target move appreciably between pulses (the frozen ocean approximation), the system should be functionally equivalent to the multifrequency system. The system does differ in an important physical aspect, in that the multifrequency CW system lays down an actual interference pattern in space through which the target moves. Although an equivalent interference pattern exists for the PDK as a result of nonlinear processing in the receiver, opinion differs as to whether the PDK case yields the same results as does the CW case.

A direct demonstration of the fact that scattering occurs from the roughness accompanying the internal waves is given by Figure 16. Shown is a time series of the X-band delta-k scatter from a passing group of wake waves taken with a radar footprint small enough to resolve individual internal waves. The dimensions of the fan-beam footprint are 10 m in azimuth and 16 m in range. Significant scattering occurs from the area roughened by the internal waves. This scattered signal shows a modulation depth of about 10 dB and a reduced level of backscatter from the surface between internal wave signatures. It is expected that several of the difference frequencies could be combined to increase further the matching signals and reduce the nonmatching noise; this will be attempted in the near future. The associated single-frequency modulation in radar cross section (not shown) is 3 to 5 dB.

Radar Scattering Calculations

The physics of the interaction between internal waves and surface waves is now reasonably well understood, at least for ocean wavelengths greater than 20 cm or so.[5] The mathematical description is given in terms of the wave action equation; the surface wave growth and decay are described by a relaxation-time approximation. The output of this calculation is the perturbed surface wave spectrum, $S(\mathbf{k};\mathbf{x},t)$. The perturbation away from an equilibrium wind-wave spectrum is caused by both the near-surface internal wave current, $u(x, y, z = 0, t)$,

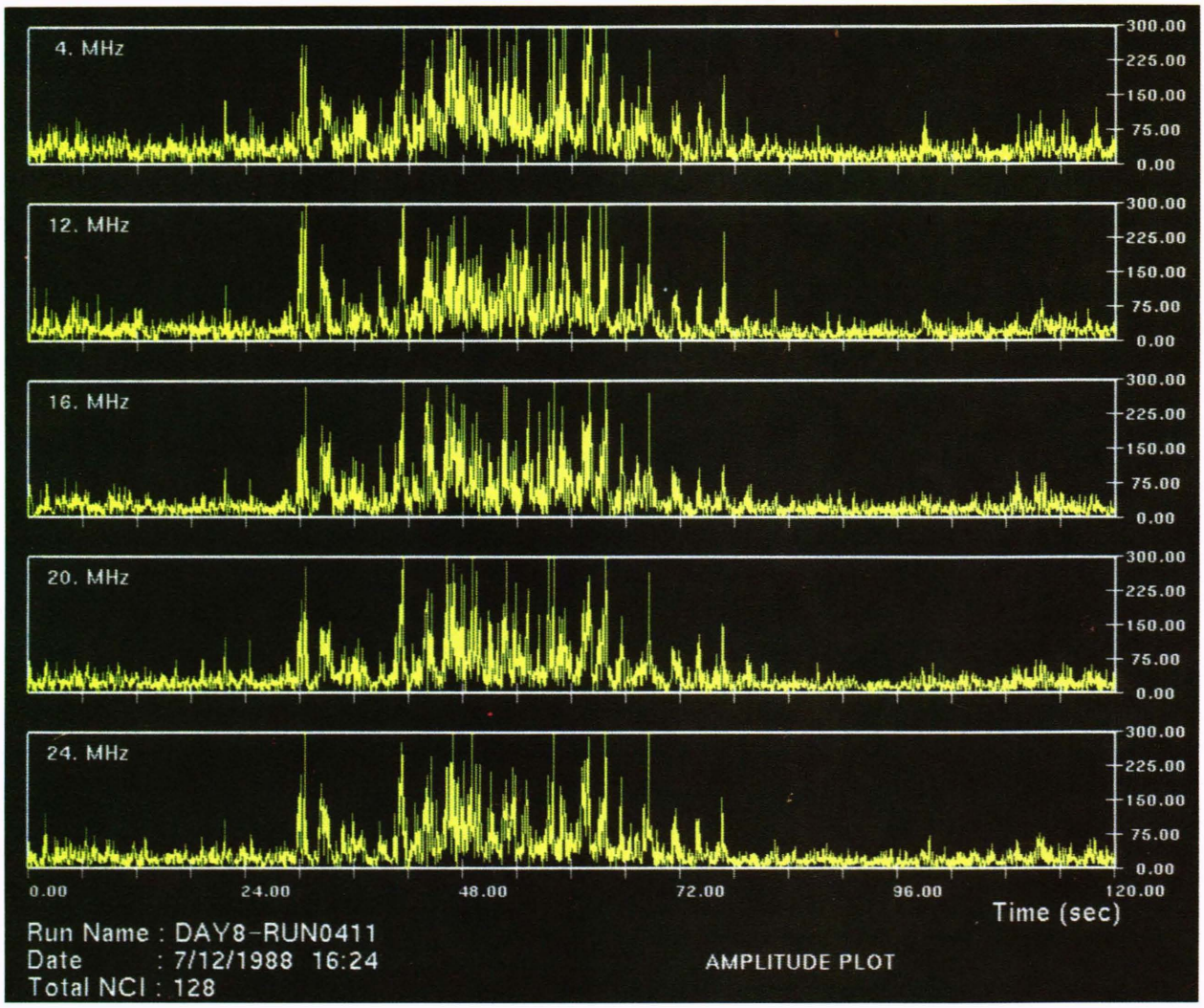

Figure 16. Time variations in backscatter observed in five delta-k channels at X band, as the internal wave crest moves through the 10-m by 16-m footprint. One wake crest lies within the radar beam from approximately 30 s to 78 s. (Illustration provided by Metratek, Inc.).

and its surface strain rates, $\partial u/\partial x$ and $\partial u/\partial y$. Here, u is the component of horizontal current in the direction of wave propagation. Both the current and its surface strain rates enter into the wave action equation. The perturbed spectrum is a slowly varying function of $\mathbf{k}$, and the largest perturbation occurs near $2\pi/k \approx 1$ to 2 m, as mentioned before. The spectrum is modulated in both space and time because of the variable internal currents. The article by Gasparovic et al. elsewhere in this issue gives an example of the methods used to calculate such perturbations.

The theory of radar backscatter from the ocean has been applied to internal wave surface signatures in recent years,[6] and considerable progress has been made in the agreement between backscatter calculations and increasingly refined field measurements. Given a perturbed surface wave spectrum, the modulation in radar scatter caused by the perturbations may be calculated by using improved versions of the Kirchhoff scattering integral. Such calculations have been carried to the point that, for frequencies from L band to X band, they are considered quite reliable.[5] At either lower or higher frequencies, however, the calculations have not as yet been verified experimentally. Extant theory has been applied with fair success to the Sognefjord data in the cases examined to date, as the following shows.

Figure 17 illustrates calculated currents and normalized radar modulations for C, X, and W bands for one particular internal wave wake. The experimentally determined amplitudes of six oscillations from Run 6 on 12 July 1988 have been fitted with model functions for ease of computation, and the scattering integrals have been evaluated numerically along a path approximately 200 m from, and parallel to, the ship track. It may be seen that the theory predicts an X-band modulation of the backscatter from the leading crest of about 10%, whereas the sixth arm is calculated to cause modulation of only a few percent.

SUMMARY AND CONCLUSIONS

The two-week-long Sognefjord experiment was conducted with radar and *in situ* observations of a canoni-

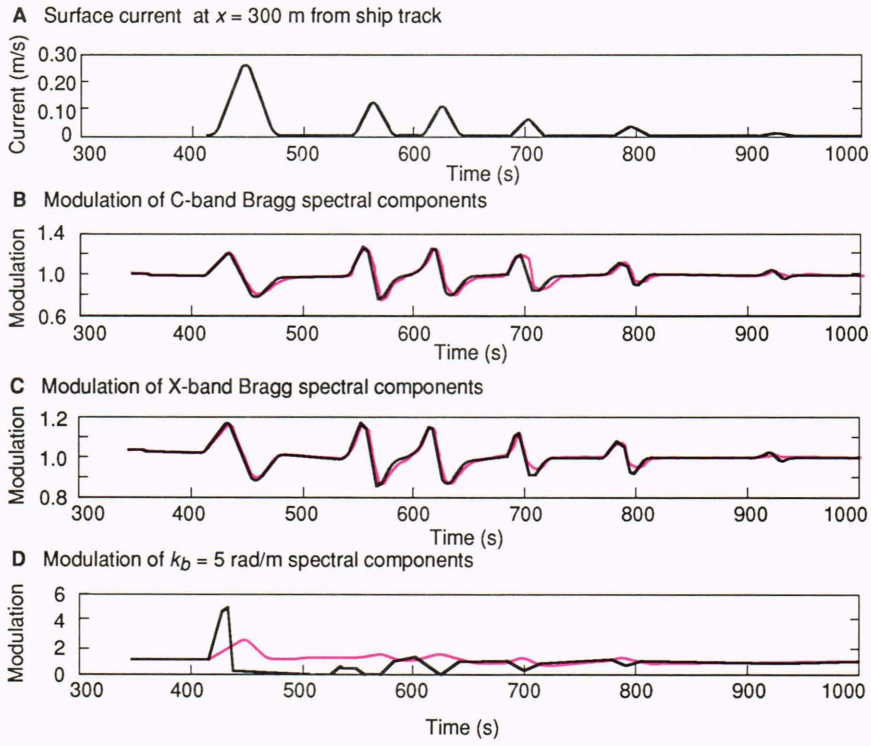

Figure 17. Calculated currents and backscatter variations at C, X, and W bands for six internal wave crests.

cal internal wave wake generated by a 51-m-long vessel in sharply stratified summer fjord waters. Coherent internal waves were generated in the measurement area that had periods from 70 to 30 s, double amplitudes ranging downward from about 1.5 m, and phase velocities between 30 and 70 cm/s. The visible internal wake crests extended at least 2 km astern of the wave-making ship. One arm of the internal wake was arranged to propagate toward several radars mounted at an elevation of 800 m on the moutainside or suspended from high-voltage transmission lines traversing the fjord. The wake signals were clear to the eye, to video cameras, and to the radars, in wind speeds up to 10 m/s (20 kt) and in light-to-moderate rain.

Subsurface and surface hydrodynamic measurements provided ground truth for the radars. Data available to define the hydrodynamic fields in the experiment area included density profiles; surface wave height and slope spectra; observations of both internal currents and longer-term, larger-scale currents; and conductivity–temperature–depth time series. Surface meteorological measurements supported the *in situ* observations.

Theoretical models of internal wave wakes were improved and applied to the data, allowing the wake properties to be integrated and extended away from the observation area. The combined observational and theoretical internal wave wake, evaluated at the surface, permitted theoretical calculations of radar scatter to be made. Doppler spectra were derived from both the observations and the models; such spectra were evaluated for both single-frequency and multifrequency delta-k modes. It was shown that the radar scatter and the spectra could be understood in terms of extant theories for the subject.

The CW multifrequency delta-k radar appears to function conceptually as a matched illumination, delta-k Bragg-like device that results in an enhanced signal-to-clutter ratio when several of its difference wavelengths match the wavelengths of the internal wave targets. The pulsed multifrequency X-band radar appears to match with surface wave scales within a single internal wave crest, rather than across several crests. Time-domain signal-to-clutter ratios in excess of 10 dB are seen in modulated delta-k returns from spatially resolved internal wave crests. The same case processed as a single frequency shows only a few decibels of modulation.

The next three articles in this issue contain more extended discussions of several aspects of the Sognefjord delta-k experiment. First, Dysthe and Trulsen treat the subsurface hydrodynamics of the internal wake and compare their calculations with experimental data. Jensen develops a theoretical foundation for the intuitive delta-k concepts presented here and also presents analyses of multiple-frequency data that show something of the efficacy of the method. Then, Thompson presents calculations of internal wave/surface wave hydrodynamic modulations and single-frequency radar backscatter therefrom. Finally, the article by Gasparovic et al., although directed toward the Loch Linnhe synthetic aperture radar experiment of 1987, contains additional material on internal wave wakes in a fjord environment that is relevant here.

REFERENCES

[1] Plant, W. J., "Studies of Backscattered Sea Return with a CW, Dual-Frequency, X-Band Radar," *IEEE Trans. Antennas Propag.* **AP-25**, 28–36 (1977).

[2] Gjessing, D. T., *Target Adaptive Matched Illumination Radar: Principles and Applications*, Peter Peregrinus, Ltd., London (1986).

[3] Gjessing, D. T., and Hjelmstad, J., "Ocean Waves and Turbulence as Observed With an Adaptive Coherent Multifrequency Radar," *J. Geophys. Res.* **91**, 2461–2475 (1986).
[4] Keller, J. B., and Munk, W. H., "Internal Wave Wakes of a Body Moving in a Stratified Fluid," *Physics of Fluids* **13**, 1425–1431 (1970).
[5] Thompson, D. R., "Intensity Modulations in Synthetic Aperture Radar Images of Ocean Surface Currents and the Wave/Current Interaction Process," *Johns Hopkins APL Tech. Dig.* **6**, 346–353 (1985).
[6] Holliday, D., St-Cyr, G., and Woods, N. E., "A Radar Ocean Imaging Model for Small to Moderate Incidence Angles," *Intl. J. Remote Sensing* **7**, 1809 (1986).

ACKNOWLEDGMENTS—The authors gratefully acknowledge the contributions of their many colleagues in the conduct of the Sognefjord experiment and in the analyses. They also acknowledge, with thanks, the support of Ronald Repka at the Defense Advanced Research Projects Agency and Inge Johansen of the Royal Norwegian Council for Scientific and Industrial Research.

THE AUTHORS

JOHN R. APEL's biography can be found on p. 294.

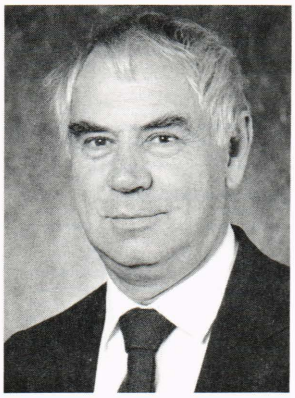

DAG T. GJESSING heads the Environmental Surveillance Technology Program, Royal Norwegian Council for Scientific and Industrial Research, Kjeller, Norway, and is also Professor of Physics at the University of Tromsø, Norway. He received degrees from Bergen University and London University (electrical engineering, 1954), and a graduate degree in geophysics from Oslo University in 1964. He was previously chief scientist at the Norwegian Defence Research Establishment, Kjeller, Norway, and has also done research for Stanford University. For the last four years, he has spent one month every fall as a visting scientist at APL. He is a member of various international scientific organizations, and he was president of the International Scientific Radio Union, Commission F on Remote Sensing and Propagation. He has written about 200 papers on radiogeophysics and is the author of *Remote Surveillance by Electromagnetic Waves for Air–Water–Land* (1978) and *Adaptive Radar in Remote Sensing* (1981).